Nanoscale

Accepted Manuscript

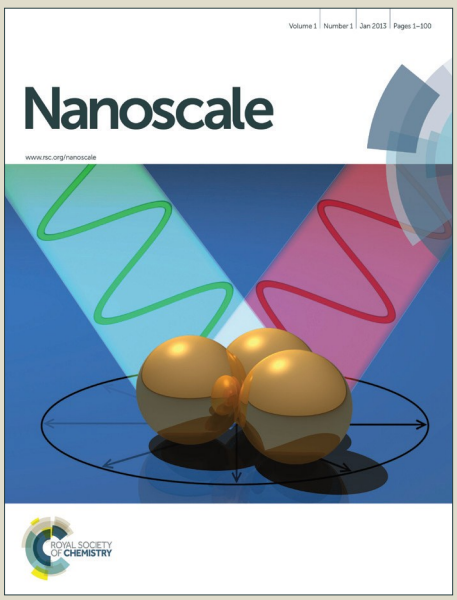

ROYAL SOCIETY OF CHEMISTRY

www.rsc.org/nanoscale

Nanoscale

ARTICLE

Supersaturation-controlled surface structure evolution of Pd@Pt core-shell nanocrystals: enhance the ORR activity at sub-10 nm scale

Received 00th January 20xx,
Accepted 00th January 20xx

DOI: 10.1039/x0xx00000x

www.rsc.org/

Kun Qi, Weitao Zheng* and Xiaoqiang Cui*

Here, we designed and implemented a facile strategy for controlling the surface evolution of Pd@Pt core-shell nanostructures by simply adjusting the volume of OH^- to control the reducing ability of ascorbic acid and finally manipulate the supersaturation in the reaction system. The surface structure of the obtained Pd@Pt bimetallic nanocrystal transformed from a Pt {111} facet-exposed island shell to a conformal Pt {100} facet-exposed shell by increasing the pH value. As-prepared well aligned Pd@Pt core-island shell nanocubes present both significantly enhanced electrocatalytic activity and favorable long-term stability toward oxygen reduction reaction in alkaline media.

1. Introduction

Platinum is a key component as the catalyst for the oxygen reduction reaction (ORR) because of the hardly exceeded efficiency.[1-3] As one of the scarcest noble metals on earth, however, its availability has become a major concern for the sustainable applications.[4] For several decades, researchers have been actively searching for alternative strategies simultaneously increasing the dispersion and enhancing their specific activity to reduce the Pt loading.[5] To this end, a great number of pioneering work had been established for Pt-based bimetallic nanostructures by deposition of Pt atoms as ultrathin shells on the surfaces of nanoparticles (NPs) made of a less expensive metal.[6-8] In general, for the epigrowth of Pt, previously layer-by-layer deposition strategies depended on the balance between the rates of surface diffusion and atom deposition, which were controlled by the reaction temperature and precursor injection rate respectively.[9] Although the core-shell nanostructures were obtained by this method, the complexity of controlling the high temperature and slow injection may inhibit the large scale synthesis and further applications.[10] Additionally, the morphology of core-shell nanostructure was confined to the shape of the seeds by this conformal overgrowth method that limited the modulation of surface structure.[11] Therefore, a much more facile and diversified method for Pt deposition is urgently required.

Recently, the theory of supersaturation has been proposed to be an effective method for nanocrystal surface structure modulation by tuning the exposed crystal facets.[12, 13] As is well known, supersaturation was defined as the variation between the chemical potentials of solute in solution and solid crystal, which can be expressed by the Thomson-Gibbs equation:[14, 15]

$$\Delta\mu = \mu_l - \mu_c = 2\sigma v / h$$

where μ_l and μ_c are the chemical potentials of solute in solution and solid crystal respectively, σ is the specific surface energy of crystalline, v is the volume of single building block and h is the size of the crystallites. While v and h are constant, briefly, higher supersaturation will finally result in the formation of crystallites with higher surface-energy facets. Taking the aforementioned consideration, because of the reduction rate of Pt precursor by AA is highly dependent on the pH value of the growth solution[16], controlling pH values and consequently controlling the supersaturation provides a potential strategy for the surface structure modulating the epigrowth of Pt-based nanocatalysts.

Herein, we designed and implemented a facile strategy for controlling the surface structure evolution of Pd@Pt core-shell nanocubes (NCs) by simply adjusting the volume of OH^- to control the reducing ability of L-ascorbic acid (AA) and finally to adjust the supersaturation in the reaction system. The surface structure of the obtained Pd@Pt bimetallic nanocrystal transformed from a Pt {111} facet-exposed island shell to a conformal Pt {100} facet-exposed shell at sub-10 nm scale by increasing the pH value. The Pd@Pt core-island shell NCs exhibited great enhancement of both specific and mass activities for ORR in comparison with commercial Pt/C catalyst, meanwhile possess favorable stability during the reaction process. Our results demonstrate a strategy via supersaturation theory for designing excellent fuel cell catalysts.

Department of Materials Science, Key Laboratory of Automobile Materials of MOE and State Key Laboratory of Superhard Materials, Jilin University, Changchun 130012 People's Republic of China.
Electronic Supplementary Information (ESI) available: [details of any supplementary information available should be included here]. See DOI: 10.1039/x0xx00000x

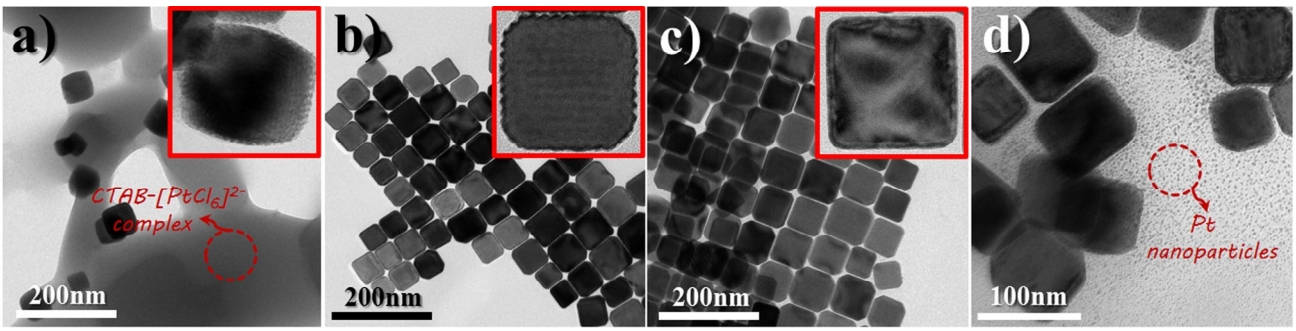

Figure 1. Typical TEM images of Pd@Pt binary nanocrystals prepared by adding different volume of 1 M KOH in the growth solution: (a) 0.00 mL, (b) 0.05 mL, (c) 0.50 mL, (d) 1.00 mL. The inset red circle of (a) shows the CTAB-$[PtCl_6]^{2-}$ complex; The inset red circle of (d) shows the Pt nanoparticles formed by self-nuclearation; The inset squares of (a), (b) and (c) show the typical singular Pd@Pt nanocrystal.

2. Result and discussion

2.1 Supersaturation-controlled surface structure evolution and characterization

Pd-Pt binary nanostructures were prepared by a seed mediated epitaxial growth method in aqueous solutions. First, Pd NC seeds were synthesized and characterized according to a previous report (Figure. S1).[17] The seed mediated growth was performed in a solution containing Pd NC seeds, cetyltrimethyl ammonium bromide (CTAB), chloroplatinic acid hexahydrate (H_2PtCl_6), and varying amount of KOH in a water bath of 40 °C (See supporting information for details). Transmission electron microscopy (TEM) images of the final product show that varying the amount of KOH exhibits an obvious effect on the morphology transformation (Figure 1). With the absence of KOH, a small amount of inhomogeneous Pd-Pt binary nanostructures were obtained with the simultaneously appearance of the abundant CTAB-$[PtCl_6]^{2-}$ complex (Figure 1a; for detail characterization and discussion, see Figure S2).[18, 19] By adding 0.05 mL of KOH, the overgrowth of Pt with a grid-like islands extending from the Pd NC surface is observed (Figure 1b and Figure S3).[20] Further increasing the volume of KOH to 0.50 mL leads to the highly uniform Pd@Pt core-shell NCs with Pt shell conformal overgrowth (Figure 1c). When 1.00 mL of KOH were injected, besides the conformal overgrowth of Pt shell, small-sized Pt nanoparticles were also formed by self-nucleation due to the fairly high supersaturation as shown in Figure 1d.[21] The dramatic transformation of the morphology from Pd@Pt core-island shell NCs to Pd@Pt core-conformal shell NCs by varying the supersaturation shows an interesting phenomenon that has never been reported previously.

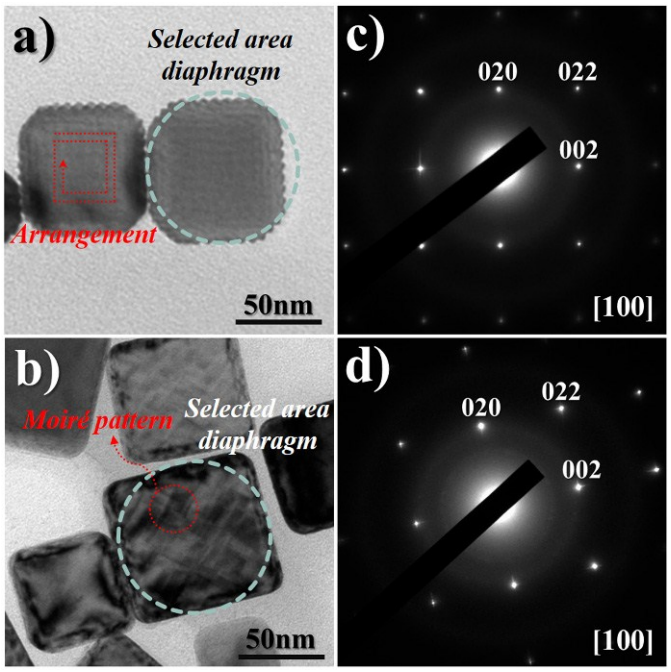

Figure 2. TEM images and corresponding SAED patterns of (a, c) Pd@Pt core-island shell NCs and (b, d) Pd@Pt core-conformal shell NCs. Inset of (a) shows the neatly aligned Pt nanoislands on Pd NCs, inset of (b) shows the Moiré pattern indicating the core-shell structure of Pd@Pt NCs

The crystalline structures were further investigated by selected area electron diffraction (SAED), energy-disperse X-ray (EDX) spectrum, and high resolution transmission electron microscopy (HRETM). Pt nanoislands exhibit a near arrangement on the surface of Pd NCs as shown in Figure 2a; however, the obvious Moiré pattern reveals a conformal overgrowth of Pt shell on Pd NCs as shown in Figure 2b.[22, 23] The single diffraction patterns of the Pd@Pt core-shell NCs (both island and conformal) clearly reveal the epitaxial, single-crystalline nature of the overgrowth (Figure 2c, 2d). The d-spacing obtained from SAED patterns of the core-shell NCs with Pt epigrowth (1.96 Å) is larger than that from the pure Pd nanocubes (1.93 Å) which is induced by the larger lattice

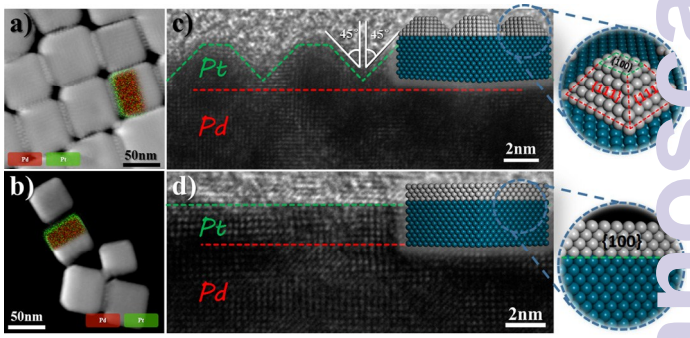

Figure 3. STEM, elemental mapping, and HRTEM images of Pd@Pt core-island shell NC (a,c) and Pd@Pt core-conformal shell NCs (b, d).

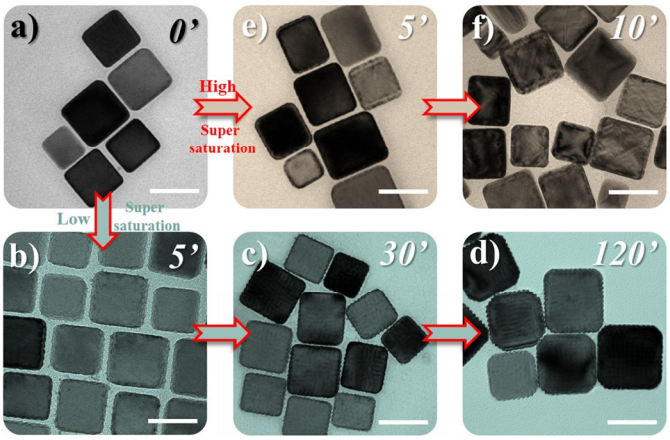

Figure 4. Typical TEM images of (a-d) Pd@Pt core-island shell NCs and (a, e-f) Pd@Pt core-conformal shell NCs with different reaction time. Scale bars all refer to 50 nm.

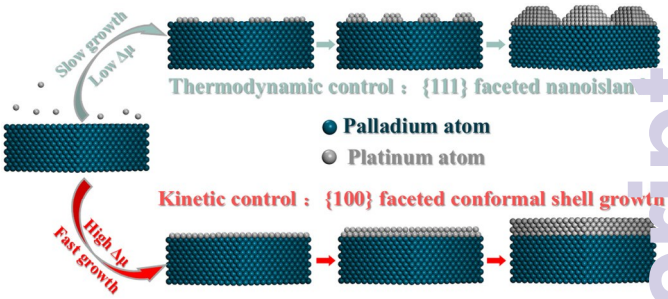

Scheme 1. Supersaturation-dependent typical diagrams for the evolution of Pd@Pt core-island shell NCs and Pd@Pt core-conformal shell NCs.

parameters of Pt (lattice mismatch of ~ 0.77 %).[24, 25] Despite some out-of-flatness in both Pt island shell and Pt conformal shell, the epigrowth was still found to be single-crystalline; that is, constructing through epitaxial growth from the substrate rather than by particle attachment from the solution.[26] High angle annular dark field-scanning transmission electron microscopy (HAADF-STEM) and element mapping further confirm the core-shell structure of the Pd@Pt NCs (Figure 3a, 3b).[27] The surface structures of the island Pt shell and conformal Pt shell overgrowth on Pd substrates were further studied by HRTEM. As shown in Figure 3c, the Pt islands obtained at lower supersaturation show a specific, truncated pyramidal shape. The angle between <100> direction (normal to the surface of Pd NC substrate) and the side of the pyramid shaped Pt islands is measured to be of 45°. Therefore, these truncated Pt pyramids expose minor {100} facets at the upmost surface and mainly {111} facets on the four sides of the islands, as shown by the atomic model of a truncated Pt pyramidal nanoisland in the inset of Figure 3c.[20, 28] In the case of higher supersaturation, the final products are Pd@Pt core-conformal shell NCs with Pt {100} facts exposed, as indicated in Figure 3d.

2.2 Investigation of the mechanism for surface structure evolution

The growth mechanism of the Pd@Pt core-shell NCs were investigated by TEM imaging of the reaction-time-dependent morphology evolution (Figure 4). TEM snapshot started from the time point of 0 minute when ascorbic acid was added. The reaction was evaluated to be ended when no obviously morphology or structure variation was observed.[29, 30] In the reaction system with a low supersaturation, the surface of Pd NCs at 5 min appears to be rougher due to the disconnected deposition of Pt atoms (Figure 4a, 4b). With the successive deposition, small Pt nanoislands are formed at 30 min (Figure 4c). The growth of Pt nanoislands are finished at 120 min (Figure 4d). In the reaction system with a high supersaturation, core-shell structure is already formed at 5 min, the reaction is very fast and completely finished within 10 min (Figure 4e, 4f).

The growth process of Pt nanocrystals reduced by AA is described as the following two steps:

$$L\text{-ascorbic acid} + Pt_l^{4+} \rightarrow_{(r)} L\text{-dehydroascorbic acid} + Pt_l^{0} + H^+ + e^- \quad \text{step 1}$$

$$Pt_l^{0} \rightarrow_{(\Delta\mu)} Pt_c^{0} \quad \text{step 2}$$

where r is the reduction rate of Pt precursor, $\Delta\mu$ is the supersaturation of Pt atoms before and after the growth process. That is to say, Pt_l^{4+} is first reduced to the metallic atoms in solution (Pt_l^{0}) at step 1. Then metallic atoms (Pt_l^{0}) grow onto the metal crystallites (Pt_c^{0}), which is driven by the supersaturation (step 2). Obviously, the chemical potential of reduced Pt atoms in solution (μ_l) will increase with the reduction rate (r). Thus the difference of chemical potentials of Pt atoms between solution phase (Pt_l^{0}) and crystal phase (Pt_c^{0}), aka the supersaturation ($\Delta\mu$), will increase with the reduction rate which is affected by the pH value.[16] At lower pH value, the system performs lower supersaturation with a slow deposition rate, the product tends to be thermodynamically stabled {111} facets dominated Pt islands shell with lower surface energy (Specific surface free energy can be seen in Table S1 in SI).[31] At higher pH value, the supersaturation increases with increasing reaction rate, which will result in a kinetically stable {100} facets dominated Pt conformal shell with higher surface energy.[32] The atomic models for the formation mechanisms of these two kinds of Pd@Pt core-shell NCs is illustrated in Scheme 1. Further decrease (Figure 1a) or increase (Figure 1d) of the supersaturation will not result in homogeneous Pd@Pt core-shell NCs because of the limited reduction ability (Figure 1a) and the excessive high supersaturation caused the surpassing of self-nucleation energy barrier, which may induce the fast Pt self-nucleation instead of epigrowth on Pd NCs (Figure 1d).[12-1

2.3 Electrocatalytic measurements for the catalysts

The structure dependent electrocatalytic activities of Pd@Pt core-shell NCs towards ORR were investigated as shown in Figure 5. The results were compared with those of Pd NC seeds, commercial Pd/C, and Pt/C catalysts (10 wt. %, average particle size ~ 3.5 nm, TEM images of these commercial catalysts are shown in Figure S4). The electrochemically active surface area (ECSA) for each NC were calculated by measuring the coulombic charge for desorption of the monolayer hydrogen (Figure S5).

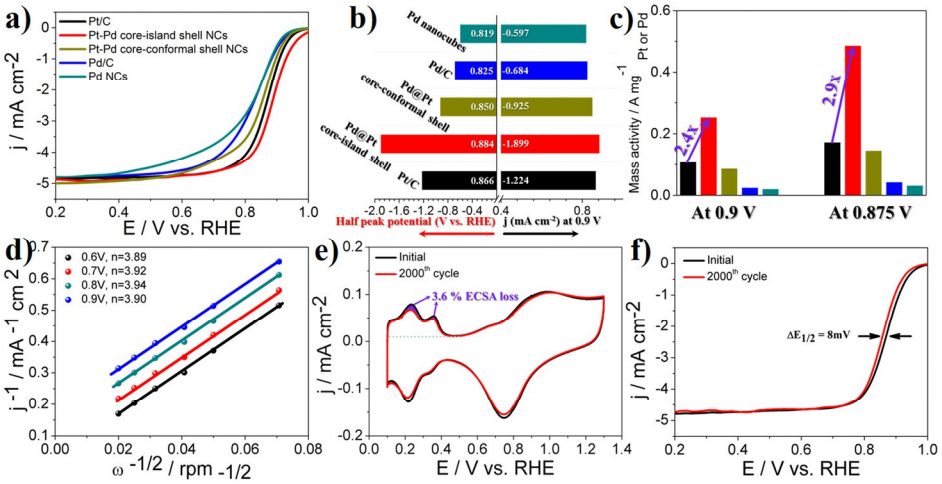

Figure 5. (a) ORR polarization curves of the Pd@Pt binary nanostructures, commercial Pd/C and Pt/C catalysts. Curves were obtained using a RDE in oxygen-saturated 0.1 M KOH at scan rate of 10 mV s^{-1} and a rotation rate of 1600 rpm. The current density was normalized by the geometric area of the electrode. (b) Histogram for half peak potential and current density at 0.9 V of the catalysts as shown in (a). (c) ORR mass activities of above mentioned Pt and Pd-based catalysts. (d) Corresponding K–L plots of Pd@Pt core-island shell NCs at different potentials. (e) Cyclic voltammetry (N_2 saturated 0.1 M KOH) and (f) Polarization curves (O_2 saturated 0.1 M KOH) of Pd@Pt core-island shell NCs before and after 2000 potential cycles.

The ORR activity was measured in an O_2-saturated 0.1 M aqueous KOH solution at room temperature with a metal (including both Pd and Pt) loading of 30 μg cm^{-2} on a rotating disk electrode (RDE) for each catalyst. The loading mass was calculated from inductively coupled plasma mass spectrometry (ICP-MS) data as shown in Table S2. Figure 5a presents the positive-going linear sweep voltammograms (LSVs) for the catalysts with a RDE rotation speed of 1600 rpm. Both Pd@Pt core-island shell NCs and Pd@Pt core-conformal shell NCs show better ORR catalytic activity than pure Pd-based catalysts (Pd NCs seeds and commercial Pd/C catalysts). It is worth noting that Pd@Pt core-island shell NCs even show a better ORR activity than Pt/C with a 18 mV positive shift on half-wave potential ($E_{1/2}$), 55 % increasement of specific activity at 0.9 V (Figure 5b), 2.4 times enhancement at 0.9 V and 2.9 times enhancement at 0.875 V for mass activity (Figure 5c). Corresponding K–L plots of Pd@Pt core-island shell NCs at different potentials indicated it exhibits a $4e^-$ transfer pathway for ORR (Figure 5d and Figure S6).[34] Such an enhancement in both specific and mass activity could be attribute to a combination for the enlargement in proportion of the ORR active Pt {111} facets on the surface and the synergistic effect between Pd and Pt by the characteristic core-shell structure.[35] Previous density functional theory (DFT) calculations and experimental measurements reported that Pt {111} facets are more active than both {100} and {110} facets towards ORR because of its appropriate oxygen adsorption and intermediate desorption free energy.[36, 37] While the fact that small Pt nanoparticles in the Pt/C catalyst were likely enclosed by a mix of {100}, {111} and {110} facets,[10] the Pd@Pt core-island shell NCs were mainly enclosed by {111} facets in addition to the minor presence of {100} facets at the top sites. Previous DFT calculations showed that the Pd core could also weaken the binding of OH^- on the surface of the catalyst by modulating the electronic structure of Pt shell, thus leading to the acceleration of ORR kinetics.[38] Meanwhile, the surface Pt atoms are more dispersed in the Pd@Pt core-island shell structure at sub-10 nm scale than those in core-shell structure, which contributes to more effective atom utilization for the improvement of ORR activity.[39]

In addition to the assessment of catalytic activity, we carried out an accelerated durability test (ADT) to evaluate the stability of Pd@Pt core-island shell NCs. To evaluate the ECSA loss during scanning, the test was conducted by applying cyclic voltammograms at a sweep rate of 0.05 V s^{-1} from 0.1 to 1.3 V in N_2 saturated 0.1 M KOH solution. A slightly ECSA loss of 3.6 % were observed after 2000th cycling (Figure 5e). The ORR long-term stability test was performed by linear potential sweep between 0.2 V and 1.0 V with a scan rate of 0.1 V s^{-1} in an O_2 saturated 0.1 M KOH solution at the RDE rotation rate of 1600 rpm. After 2000th potential cycling, only a slightly negative shift of 8 mV on $E_{1/2}$ were observed, which indicates its great ORR stability. Pd@Pt core-shell nanocrystals is better for the protection from dissolution and/or agglomeration during the durability test because of their characteristic surface structure. The Pd core is proposed to inhibit the corrosion of the Pt shell by sacrificing itself, resulting in an enhancement of the durability for ORR.[40]

3. Conclusions

In summary, we have demonstrated a facile and diversified seed-mediated supersaturation-controlled epigrowth approach for the fabrication of Pd@Pt core-shell nanostructures by adjusting the pH value in the reaction system. The formation mechanism of the Pd@Pt core-shell NCs was investigated based on the study of time-dependent morphology evolution by taking TEM snapshots during the growth process. As-prepared well aligned Pd@Pt core-island shell NCs present both significantly enhanced electrocatalytic activity and favorable long-term stability toward ORR in alkaline media. For the first time, the present work provides a facile strategy for controllable deposition of Pt on Pd substrate at sub 10-nm scale by adjusting pH and demonstrates a potential possibility via supersaturation theory for designing excellent fuel cell catalysts.

Acknowledgements

This work was financially supported by the National Natural Science Foundation of China (No. 51571100, 21275064), the Program for New Century Excellent Talents in University (NCET-

10-0433), and the Specialized Research Fund for the Doctoral Program of Higher Education (20130061110035).

Notes and references

1. J. B. Wu and H. Yang, *Acc.Chem.Res.*, 2013, **46**, 1848-1857.
2. X. Ge, A. Sumboja, D. Wuu, T. An, B. Li, F. T. Goh, T. A. Hor, Y. Zong and Z. Liu, *ACS Catal.*, 2015, **5**, 4643-4667.
3. Y. J. Sa, C. Park, H. Y. Jeong, S. H. Park, Z. Lee, K. T. Kim, G. G. Park and S. H. Joo, *Angew. Chem. Int. Edit.*, 2014, **53**, 4102-4106.
4. S. F. Xie, S. I. Choi, N. Lu, L. T. Roling, J. A. Herron, L. Zhang, J. Park, J. G. Wang, M. J. Kim, Z. X. Xie, M. Mavrikakis and Y. N. Xia, *Nano Lett.*, 2014, **14**, 3570-3576.
5. K. Sasaki, H. Naohara, Y. M. Choi, Y. Cai, W. F. Chen, P. Liu and R. R. Adzic, *Nat. Commun.*, 2012, **3,** 1151.
6. Z. M. Peng, J. B. Wu and H. Yang, *Chem. Mater.*, 2010, **22**, 1098-1106.
7. P. J. Straney, L. E. Marbella, C. M. Andolina, N. T. Nuhfer and J. E. Millstone, *J. Am. Chem. Soc.*, 2014, **136**, 7873-7876.
8. S. E. Habas, H. Lee, V. Radmilovic, G. A. Somorjai and P. Yang, *Nat Mater*, 2007, **6**, 692-697.
9. X. H. Xia, S. F. Xie, M. C. Liu, H. C. Peng, N. Lu, J. G. Wang, M. J. Kim and Y. N. Xia, *P. Natl. Acad. Sci.* , 2013, **110**, 6669-6673.
10. J. Park, L. Zhang, S.-I. Choi, L. T. Roling, N. Lu, J. A. Herron, S. Xie, J. Wang, M. J. Kim and M. Mavrikakis, *ACS Nano*, 2015, **9**, 2635-2647.
11. B. Lim, H. Kobayashi, T. Yu, J. Wang, M. J. Kim, Z.-Y. Li, M. Rycenga and Y. Xia, *J. Am. Chem. Soc.*, 2010, **132**, 2506-2507.
12. Z. M. Peng and H. Yang, *Nano Today*, 2009, **4**, 143-164.
13. M. Jiang, B. Lim, J. Tao, P. H. C. Camargo, C. Ma, Y. Zhu and Y. Xia, *Nanoscale*, 2010, **2**, 2406-2411.
14. H. X. Lin, Z. C. Lei, Z. Y. Jiang, C. P. Hou, D. Y. Liu, M. M. Xu, Z. Q. Tian and Z. X. Xie, *J. Am. Chem. Soc.*, 2013, **135**, 9311-9314.
15. Markov, I. V. Crystal Growth for Beginners: Fundamentals of Nucleation, Crystal Growth and Epitaxy; 2nd ed.; World Scientific: Singapore; River Edge, N.J., 2003.
16. M. M. Bower, C. J. DeSantis and S. E. Skrabalak, *J. Phys. Chem. C*, 2014, **118**, 18762-18770.
17. W. X. Niu, L. Zhang and G. B. Xu, *ACS Nano*, 2010, **4**, 1987-1996.
18. A. T. Hubbard and F. C. Anson, *Anal. Chem.*, 1966, **38**, 1887-1893.
19. R. Krishnaswamy, H. Remita, M. Impéror-Clerc, C. Even, P. Davidson and B. Pansu, *ChemPhysChem*, 2006, **7**, 1510-1513.
20. B. T. Sneed, C. H. Kuo, C. N. Brodsky and C. K. Tsung, *J. Am. Chem. Soc.*, 2012, **134**, 18417-18426.
21. N. Fan, Y. Yang, W. Wang, L. Zhang, W. Chen, C. Zou and S. Huang, *ACS Nano*, 2012, **6**, 4072-4082.
22. Z. Wang, Z. Chen, H. Zhang, Z. Zhang, H. Wu, M. Jin, C. Wu, D. Yang and Y. Yin, *ACS Nano*, 2015, **9**, 3307-3313.
23. M. Jin, H. Zhang, J. Wang, X. Zhong, N. Lu, Z. Li, Z. Xie, M. J. Kim and Y. Xia, *ACS Nano*, 2012, **6**, 2566-2573.
24. S. Guo, S. Dong and E. Wang, *ACS Nano*, 2009, **4**, 547-555.
25. Z. Peng and H. Yang, *J. Am. Chem. Soc.*, 2009, **131**, 7542-7543.
26. K. Qi, Q. Wang, W. Zheng, W. Zhang and X. Cui, *Nanoscale*, 2014, **6**, 15090-15097.
27. L. Zhang, L. T. Roling, X. Wang, M. Vara, M. Chi, J. Liu, S.-I. Choi, J. Park, J. A. Herron and Z. Xie, *Science*, 2015, **34**[illegible] 412-416.
28. P. Nolte, A. Stierle, N. Y. Jin-Phillipp, N. Kasper, T. U. Schu[illegible] and H. Dosch, *Science*, 2008, **321**, 1654-1658.
29. C. L. Lu, K. S. Prasad, H. L. Wu, J. A. Ho and M. H. Huang, *J. Am. Chem. Soc.*, 2010, **132**, 14546-14553.
30. D. Kim, Y. W. Lee, S. B. Lee and S. W. Han, *Angew. Chem. Int. Edit.*, 2012, **51**, 159-163.
31. C. Wang, W. D. Tian, Y. Ding, Y. Q. Ma, Z. L. Wang, N. M. Markovic, V. R. Stamenkovic, H. Daimon and S. H. Sun, *J. Am. Chem. Soc.*, 2010, **132**, 6524-6529.
32. Y. Xiong and Y. Xia, *Adv. Mater.*, 2007, **19**, 3385-3391.
33. J. W. Hong, S. W. Kang, B. S. Choi, D. Kim, S. B. Lee and S. W. Han, *ACS Nano*, 2012, **6**, 2410-2419.
34. J. Y. Chen, X. Wang, X. Q. Cui, G. M. Yang and W. T. Zh[illegible] *Chem. Commun.*, 2014, **50**, 557-559.
35. S. J. Guo, S. Zhang and S. H. Sun, *Angew. Chem. Int. Ed[illegible]* 2013, **52**, 8526-8544.
36. A. Morozan, B. Jousselme and S. Palacin, *Energy Environ. Sci.*, 2011, **4**, 1238-1254.
37. Y. Nie, L. Li and Z. Wei, *Chem. Soc. Rev.*, 2015, **44**, 216[illegible] 2201.
38. C. Koenigsmann, A. C. Santulli, K. P. Gong, M. B. Vukmirovi[illegible] W. P. Zhou, E. Sutter, S. S. Wong and R. R. Adzic, *J. Am. Chem. Soc.*, 2011, **133**, 9783-9795.
39. H. Zhang, M. S. Jin, H. Y. Liu, J. G. Wang, M. J. Kim, D. R. Yang, Z. X. Xie, J. Y. Liu and Y. N. Xia, Acs Nano, 2011, [illegible] 8212-8222.
40. V. Mazumder, M. Chi, K. L. More and S. Sun, *J. Am. Chem. Soc.*, 2010, **132**, 7848-7849.